

Volume Currents in Forward and Inverse MEG Simulations using Realistic Head Models

Robert Van Uitert, David Weinstein, and Chris Johnson

Scientific Computing and Imaging Institute
School of Computing
University of Utah

Abstract

Many magnetoencephalography (MEG) forward and inverse simulation models employ spheres, a singular shape which does not require consideration of volume currents. With more realistic, inhomogeneous, anisotropic, non-spherical head models, volume currents cannot be ignored. We verify the accuracy of the finite element method in MEG simulations by comparing its results for a sphere containing dipoles to those obtained from the analytic solution. We then use the finite element method to show that in a realistic model, the magnetic field normal to the MEG detector due to volume currents often has a magnitude on the same order or greater than the magnitude of the primary magnetic field from the dipole. Forward and inverse MEG simulations using the realistic model demonstrate the disparity in results between calculations containing volume currents and those without volume currents. Volume currents should be included in any accurate calculation of MEG results, whether they be for a forward or inverse simulation.

Keywords: Forward MEG, Inverse MEG, Source localization, Volume currents, Finite element method

Introduction

External magnetic fields produced by neuronal activity within the brain can be measured using magnetoencephalography (MEG). A standard method for modeling the activity of these neurons assumes that they act as electric current dipoles. The electric fields produced by the dipoles can be separated into two components: the primary current, which represents the area of neural activity, and the secondary or volume current, which is the electric field that results from the primary current^{7,8}. MEG detectors measure the net magnetic field due to both primary and secondary currents.

Attempts to determine the magnetic fields that result from current dipoles, the forward problem, most commonly use a model for simulations consisting of a set of concentric spheres, each with homogeneous and isotropic conductivity. Given this model, the MEG forward problem can be reduced to a closed form analytic solution. However, with more realistic, inhomogeneous, anisotropic, non-spherical head models, a closed form solution is not as easily computed and

approximation methods, such as finite or boundary element methods, must be used.

Many realistic head models used for forward simulation do not incorporate the volume currents in the MEG measured magnetic field. We used the numeric finite element method^{1,2,5,12,16} to investigate the effects that volume currents have on the total magnetic field measured at the MEG detectors, and their importance in accurately calculating magnetic fields detected by MEG. The accuracy of our numeric model is first confirmed by comparing the model's computed results for a sphere containing dipoles to that of the analytic solution for the sphere; this numeric method is then applied to forward simulations in a more realistic head model.

The task of determining the current dipole's location within the head from the normal component of the magnetic field located at each detector, the inverse problem or dipole source localization, relies on the techniques and modeling of the forward problem. After determining the importance of volume currents in the forward simulations, we used our forward model to perform inverse simulations on the realistic head model and to investigate the importance of volume currents for accurate dipole source localization.

Background

The dipole's primary current density, J_p , results from the electromotive force impressed by biological activity on conducting tissues¹¹. Assuming J_p is within a conductive region, G , of the brain with conductivity σ and that the magnetic permeability is homogeneous, $\mu = \mu_0$, the quasistatic approximations of Maxwell's equations in determining the electric field, E , and the magnetic field, B , apply as follows:

$$E = -\nabla\phi \quad (1)$$

$$\nabla \times B = \mu_0 J \quad \nabla \cdot B = 0 \quad (2)$$

$$J = J_p + \sigma E \quad (3)$$

where ϕ is the electric potential and J is the total current density. The magnetic field is calculated by the Biot-Savart law:

$$B(r) = \mu_0/4\pi \int_G J(r') \times (r - r')/|r - r'|^3 dv \quad (4)$$

where r' is the coordinate of the dipole and r is the point of detection. Combining equations (1), (3), and (4),

Address correspondence to Chris Johnson, Scientific Computing and Imaging Institute, School of Computing, University of Utah, Salt Lake City, UT 84112. Electronic mail: crj@cs.utah.edu; Robert Van Uitert, electronic mail: vauitert@cs.utah.edu; David Weinstein, electronic mail: dmw@cs.utah.edu

$$\begin{aligned}
B(r) &= \mu_0/4\pi \int_G [J_p - \sigma \nabla \phi] \times (r - r') / |r - r'|^3 dv \\
&= (\mu_0/4\pi) \int_G J_p \times (r - r') / |r - r'|^3 dv \\
&\quad - \Sigma \sigma_j \int_{G_j} \nabla \phi \times (r - r') / |r - r'|^3 dv \quad (5)
\end{aligned}$$

For a current dipole with a moment Q :

$$\begin{aligned}
B(r) &= \mu_0/4\pi [Q \times (r - r') / |r - r'|^3 \\
&\quad - \Sigma \sigma_j \int_{G_j} \nabla \phi \times (r - r') / |r - r'|^3 dv] \quad (6)
\end{aligned}$$

The integral portion of equation (6) models the volume currents which are dependent upon the conductivity and electric potential, while the balance of the right hand side of equation (6) models the primary current.

If the conductor is in the shape of a sphere, an analytic closed form equation exists for calculating the magnetic field. According to Sarvas¹¹, the magnetic field outside of a homogeneous sphere enclosing a dipole can be calculated as follows:

$$B(r) = \mu_0/4\pi F^2 (FQ \times r' - Q \times r' \cdot r \nabla F) \quad (7)$$

where $F = |a|(|r||a| + |r|^2 - r' \cdot r)$, $a = r - r'$, and $\nabla F = (|a|^2/|r| + a \cdot r/|a| + 2|a| + 2|r|)r - (|a| + 2|r| + a \cdot r/|a|)r'$.

Equation (7) shows that for a spherical conductor, if the source is oriented radially to the point where the magnetic field is being measured, then the system is a magnetically silent volume conductor³. Note that equation (7) does not directly mention conductivity, σ . However, although in a homogeneous sphere the contribution to the magnetic field from the volume currents is independent of conductivity, the volume currents are implicitly incorporated in equation (7)¹¹ and do contribute to B .

The detectors used in MEG measure only the component of the magnetic field normal to the detectors⁶. Thus equation (6) becomes

$$\begin{aligned}
B(r) &= \mu_0/4\pi [Q \times (r - r') / |r - r'|^3 \cdot n \\
&\quad - \Sigma \sigma_j \int_{G_j} \nabla \phi \times (r - r') / |r - r'|^3 dv \cdot n] \quad (8)
\end{aligned}$$

where n is the normal to the detector. Equation (7) then becomes

$$B(r) = \mu_0/4\pi F^2 (FQ \times r' - Q \times r' \cdot r \nabla F) \cdot r / |r| \quad (9)$$

Equation (9) indicates that in the spherically symmetric conductor, MEG is sensitive only to the tangential component of the primary electric current^{4,6}.

Results

In our simulations, the finite element method was used to calculate the electric potential in a discrete, numeric model of both spheres and realistic heads¹⁴. The SCIRun Problem Solving Environment⁹ was used to drive the forward and inverse MEG simulations.

Spherical Head Model

Several tests were performed to validate the numeric model being used for simulations. Using a sphere, we calculated the magnetic field by our numeric model and compared it to the magnetic field calculated by the analytic equation (7). The sphere tests were performed on a 98,001 node unit decimeter sphere containing 459,784 elements with 180 detectors placed symmetrically around the sphere at radii of 1.3dm, 1.4dm, 1.5dm, and 1.6dm. A dipole was placed first at the center of the sphere with a moment of (0,0,1). In comparing the numeric to the analytic solution, the cumulative RMS error at all the detectors was 1.12×10^{-17} T.

A dipole was next placed in the sphere at (0.8,0.5,0) with moment (1,-0.5,0). The results from the numeric model were compared to the calculations from equation (7) and were found to correspond with a correlation coefficient of 0.998. Figures 1 and 2 allow for a visual comparison between the analytic and numeric magnetic fields calculated at the 180 detectors for this dipole.

The next validation test employed dipoles that were randomly placed and randomly oriented in the sphere. Only one dipole was inside the sphere for each of the numeric and analytic magnetic field calculations, and each of these was evaluated for all 180 detectors. The calculations were performed for 100 different dipoles. The mean correlation coefficient between the calculated total magnetic field for numeric and for analytic solutions was 0.991 ± 0.014 , with no data points correlating at less than 0.914. Figure 3 indicates the correlation coefficient for each dipole.

Using the same 100 dipoles, only the radial component of the numeric solutions with and without the volume currents was compared to the radial component of the analytic solutions. The correlation coefficient for each dipole appears in Figure 4; all coefficients were greater than or equal to 0.998. The minimal difference between solutions with volume currents and without volume currents indicates that the radial component of the magnetic field due to the volume currents is close to zero in the sphere.

The numeric solutions with and without the volume currents for the total magnetic field for the same 100 dipoles were also compared to the analytic solutions. The mean correlation coefficient with the volume currents was 0.991 ± 0.014 , and without volume currents was 0.900 ± 0.066 ; the coefficient for each dipole with the volume currents and without the volume currents appears in Figure 5. A large discrepancy in accuracy between solutions including volume currents and those without volume currents is apparent when calculating the total magnetic field that was not evident when measuring the radial component alone. For each individual dipole, the correlation coefficient for solutions with the volume currents invariably was higher than was the coefficient for those without the volume currents.

Realistic Head Forward Simulation

Next, the numeric finite element method of MEG forward simulation was used on a realistic head model consisting of 72,745 nodes, 406,493 elements, and 64 detectors placed over the head. This model was constructed from a volume magnetic resonance image (MRI) scan and consisted of six conductivity values: air ($\sigma = 0.0$ S/m), skin ($\sigma = 1.0$ S/m), bone ($\sigma = 0.05$ S/m), CSF ($\sigma = 4.62$ S/m), gray matter ($\sigma = 1.0$ S/m), and white matter ($\sigma = 0.43$ S/m)¹⁰.

A dipole with moment (0,0,-1200) was located at (79,177,131), corresponding to the right posterior frontal

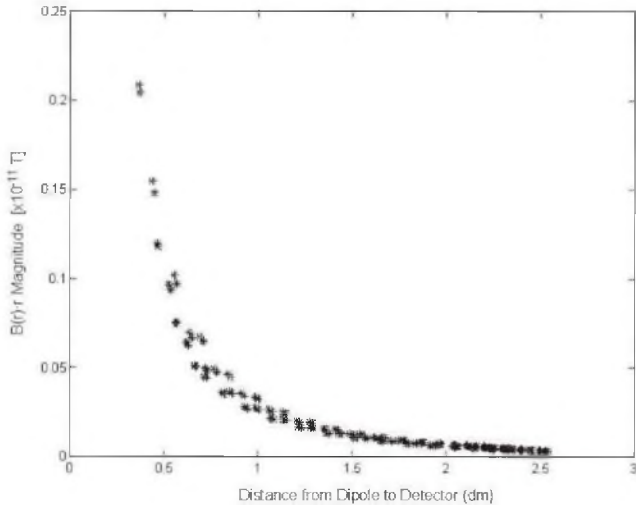


Figure 1: Analytic solution of magnitude of magnetic field at detectors for dipole at $(0.8,0.5,0)$ with moment $(1,-0.5,0)$

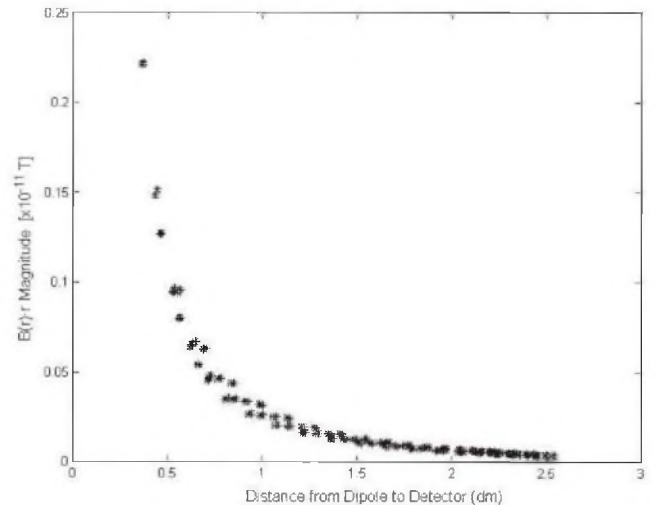


Figure 2: Numeric solution of magnitude of magnetic field at detectors for dipole at $(0.8,0.5,0)$ with moment $(1,-0.5,0)$

cerebrum. At 61% of the detectors (39 out of 64), the normal component of the magnetic field due to the volume currents was of the same order of magnitude or larger than the normal component of magnetic field due to the primary current. At 16% of the detectors (10 out of 64), the normal component of the magnetic field due to the volume currents was at least an order of magnitude greater than the magnetic field due to the primary current. Figure 6 shows the magnitude of the magnetic field normal to the detector at each of the detector positions with the magnetic field due to the combined volume currents and primary currents, with the magnetic field due to the primary currents alone, and with the magnetic field due to the volume currents alone. Detectors numbered 1-18 measure fields over the left frontal region, detectors numbered 19-29 were localized over the left occipital parietal region and were the most remote from the dipole, detectors numbered 30-41, were placed over the right parietal occipital region, and detectors numbered 42-64 were localized over the right frontal region and were the closest to the placement of the dipole in this model.

A dipole was also placed at $(150,150,50)$, in the left parietal lobe, with moment $(0,0,-1200)$. At 77% of the detectors (49 of 64), the normal component of the magnetic field due to the volume currents was of the same order of magnitude or larger than the normal component of the magnetic field due to the primary current. At 13% of the detectors (8 of 64), the normal component of the magnetic field due to the volume currents was at least an order of magnitude greater than the magnetic field due to the primary current. Figure 7 shows the magnitude of the magnetic field normal to the detector at each of the detector positions with the magnetic field due to the combined volume currents and primary currents, with the magnetic field due to the primary currents alone, and with the magnetic field due to the volume currents alone. The detectors for this simulation were at the same position as were the detectors for the simulation with the dipole in the right posterior frontal cerebrum.

Realistic Head Inverse Simulation

The normal component of the magnetic field was calculated at each detector for a specific dipole using a forward simulation; the detectors' magnetic field data for this dipole, but not the dipole's location, was then used as the "measured" data with which to run an inverse MEG simulation. The inverse simulation was performed by positioning a test dipole in one element of the finite element head mesh, finding the optimal magnitude and orientation for the dipole in that element using linear least squares optimization, and then computing the error between the forward solution for the test dipole and the "measured" data^{13,15}. The test dipole was then moved to different positions in the mesh until a position was found where the error between the forward solution for the test dipole and the "measured" data was minimized. Rather than calculating the error between the forward solution for each test dipole position and the "measured" solution in each element, we used the downhill simplex⁸ optimization search technique which requires the evaluation of fewer elements to find the position where the minimum error occurs between the forward calculated solution and the "measured" solution.

Figure 8 shows the calculated location of the dipole for an inverse MEG simulation using our realistic head model with the simulated "measured" data being for a dipole at the location $(79,177,131)$ in the right posterior frontal area. Ten inverse simulations were run with the same "measured" data as was used in Figure 8 but by starting the search at different positions within the head. 90% (9 of 10) of these simulations localized the dipole source to within 5mm of the correct location, with the closest distance being 0mm away from the correct location and the greatest distance being 18mm. The average error in correctly identifying the dipole location in the 10 trials was 4.0 ± 5.1 mm.

Finally, inverse MEG simulations were performed on data "measured" at detectors for 10 different dipole locations within our realistic head model. Two sets of simulations were run; one set took into account the magnetic fields due to both the primary and volume currents, and the other set used only the magnetic field resulting from the primary cur-

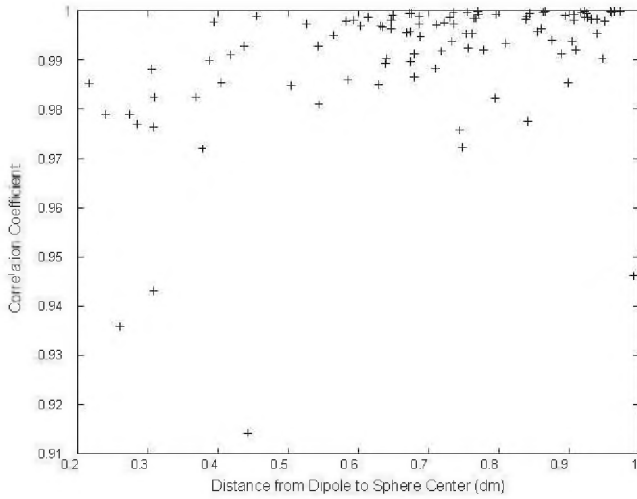


Figure 3: Correlation coefficient of numeric to analytic calculations for total magnetic field versus distance from dipole to sphere center (100 randomly placed and oriented dipoles)

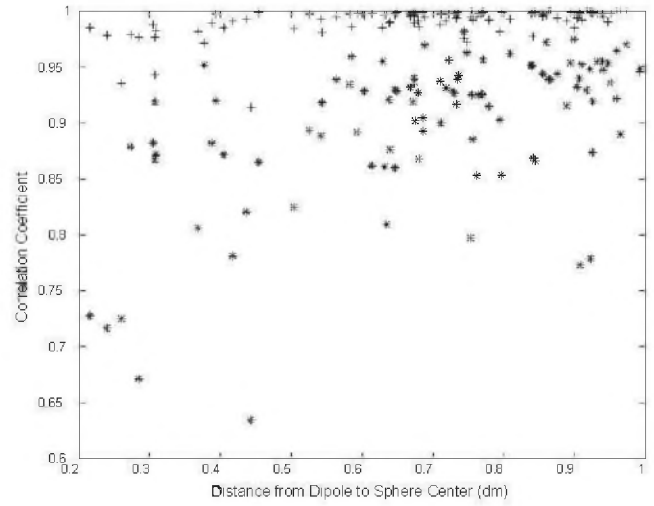


Figure 5: Correlation coefficient versus distance from dipole to sphere center for total magnetic field (100 randomly placed and oriented dipoles): crosses indicate numeric solution with volume currents, and stars indicate numeric solution without volume currents

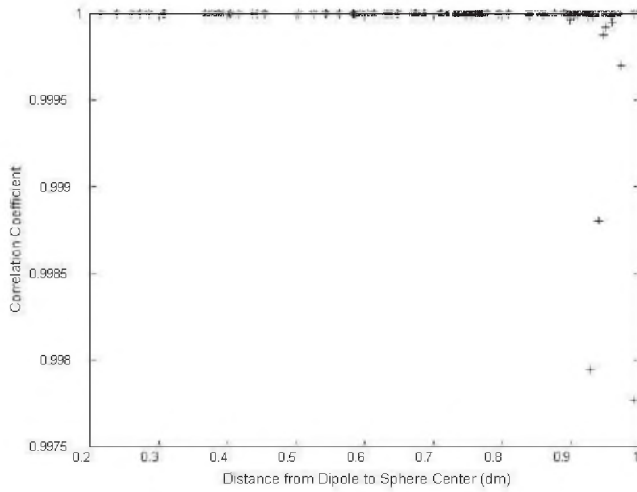


Figure 4: Correlation coefficient versus distance from dipole to sphere center for radial component of magnetic field (100 randomly placed and oriented dipoles): crosses indicate numeric solution with volume currents, and stars indicate numeric solution without volume currents

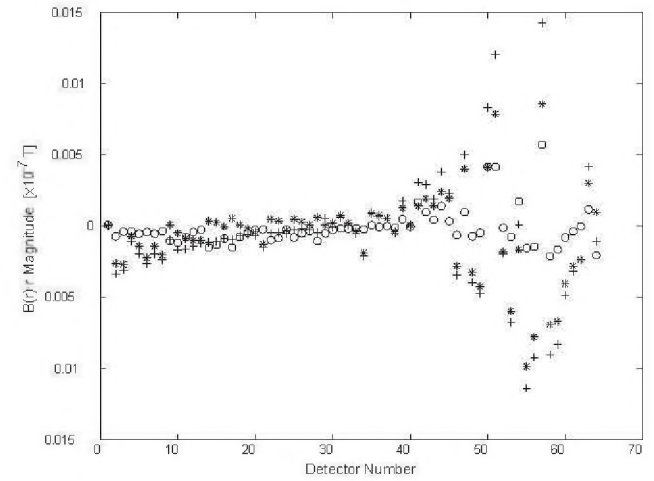


Figure 6: Normal component of the magnetic field for each detector with dipole in right posterior frontal cerebrum: crosses indicate numeric solution with volume currents and primary currents, stars indicate numeric solution with primary currents alone, circles indicate numeric solution with volume currents alone

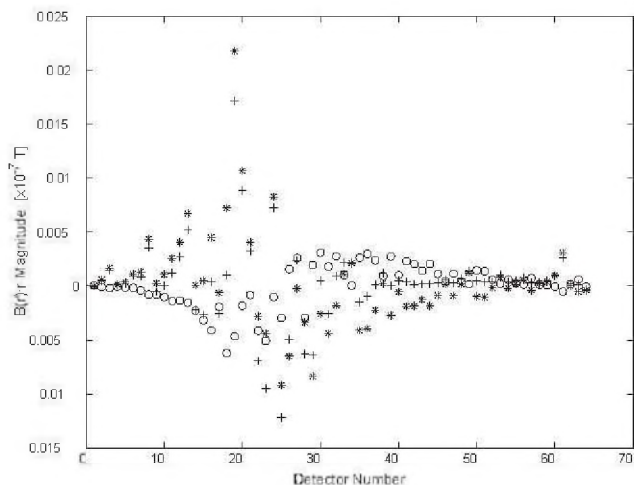


Figure 7: Normal component of the magnetic field for each detector with dipole in left parietal lobe of the brain: crosses indicate numeric solution with volume currents and primary currents, stars indicate numeric solution with primary currents alone, circles indicate numeric solution with volume currents alone

rent and ignored that due to the volume current (Table 1). Figure 9 shows the dipole source localization point for the inverse solution obtained using the “measured” data for a dipole at location (150,150,50) in the left parietal lobe of the brain; the magnetic fields for both the primary and volume currents were used in this simulation. Figure 10 shows the dipole source localization point for the inverse solution obtained using the same “measured” data as was used in Figure 9, except that the simulation in Figure 10 does not include the magnetic field due to volume currents in the calculation. In the ten dipole source localizations, 70% (7 of 10) of the localizations performed without volume currents resulted in a solution inaccurate by 7mm or greater, whereas 90% (9 of 10) of the localizations performed using the magnetic fields due to both primary and volume currents were within 6mm of the correct dipole location. The average error in correctly identifying the dipole location for trials which included the magnetic field due to volume currents was $3.2 \pm 2.2\text{mm}$; the average error for trials not taking into account the magnetic field due to volume currents was $23.8 \pm 27.0\text{mm}$.

Discussion

The tests performed with the spheres and the comparison of the results with those obtained using the analytic solutions show that our numeric model works accurately. The RMS error due to the dipole placed at the origin with moment (0,0,1) was only $1.12 \times 10^{-17}\text{T}$; this discrepancy is due to the finite element approximation error. Further confirmation of the numeric model’s accuracy is the results obtained with the dipole at (0.8,0.5,0) with moment (1,-0.5,0) (Figures 1 and 2). The detectors closest to the dipole location have the highest magnitude of magnetic field, whereas those farther away have a smaller magnitude, as would be expected. The numeric and analytic solutions correlate highly (coefficient = 0.998).

The mean correlation coefficient of the 100 randomly

placed and oriented dipoles, 0.991 ± 0.014 , further indicates the accuracy of our model. As can be seen in Figure 3, only 4 of the 100 dipoles have a correlation coefficient less than 0.946. The errors that do occur stem from finite element approximation.

Figure 4 shows the correlation coefficient of our model with the analytic solution when calculating the normal component of the magnetic field generated by randomly placed and oriented dipoles in a sphere. The error with and without the volume currents is the same except for 11 detectors; the differences at these 11 detectors, the smallest of which is a correlation coefficient of 0.998, are based solely on finite element approximation error and increase as the distance from the center of the sphere increases because the spherical mesh employed was only an approximation containing an imperfect jagged boundary. The virtually identical results obtained with and without taking into account the volume currents is expected because, as demonstrated in Hämäläinen et al.⁴, the normal component of the magnetic field for a sphere results from only the tangential component of the primary current.

In contrast to calculations involving only the normal component of the magnetic field, Figure 5 clearly indicates the importance of volume currents in total magnetic field calculations. The correlation coefficient when comparing the magnetic fields calculated with both primary and volume currents to the analytic solution averaged 0.991 ± 0.014 , with 96% of the dipoles above 0.946. The correlation coefficient for the solution without volume currents averaged 0.900 ± 0.066 , with 79% of the dipoles having a correlation coefficient less than 0.946.

The above tests demonstrate that our numeric model is reasonably accurate and that the small inaccuracies that do occur result from finite element approximation. Using a numeric finite element method on a homogeneous, isotropic sphere is only a test case, however; the true usefulness of this technique becomes apparent when the method is applied to a realistic head which incorporates varying conductivities and for which an analytic solution is not available. The realistic model reemphasizes the importance of including volume currents in MEG calculations, as at least 61% of the detectors in our model measured magnetic fields due to volume currents that had magnitudes as large as or greater than the magnetic fields due to primary currents, and at least 13% of the detectors measured magnetic fields due to volume currents that were over an order of magnitude greater than the magnetic fields due to primary currents.

Figures 6 and 7 show the importance of using return currents when calculating magnetic field strengths in realistic head models. In Figure 6, the increase in absolute magnitude of the calculated magnetic field occurred at detector numbers 42-64 which were located on the right posterior frontal portion of the head and were closest to the dipole location. Similarly, the increase in the absolute magnitude of the calculated magnetic field at detector numbers 10-29 in Figure 7 reflect the fact that these detectors were located on the left parietal portion of the head and were closest to the dipole in this trial. In accord with the Biot-Savart law (4), the positive or negative magnitude of the magnetic field at each detector depends on the position of the detector with respect to the dipole. Figures 6 and 7 show that, for detectors close to the location of a dipole, the magnitude of the magnetic field would be calculated incorrectly for both positive and negative orientations if only the magnetic fields due to the primary currents were included. For detectors remote from the dipole, such as detectors numbered 19-29

Trial Number	Dipole Coordinates & Location in Brain	Error With Volume Currents Magnetic Field	Error Without Volume Currents Magnetic Field
1	(79,177,131) – Right Posterior Frontal	5mm	12mm
2	(150,150,50) – Left Parietal	3mm	62mm
3	(100,150,100) – Right Temporal	1mm	8mm
4	(150,170,150) – Left Frontal	8mm	8mm
5	(100,150,100) – Right Temporal*	7mm	46mm
6	(79,150,50) – Right Parietal	2mm	76mm
7	(100,220,100) – Right Precentral Gyrus	4mm	4mm
8	(100,110,50) – Right Occipital	1mm	14mm
9	(142,224,112) – Left Mid Frontal	2mm	4mm
10	(70,200,112) – Right Mid Frontal	1mm	4mm

* – had different orientation from previous right temporal dipole

Table 1: Dipole coordinates and position in brain, error in inverse localization calculations including the magnetic field due to volume currents, and error in inverse localization calculations excluding the magnetic field due to volume currents

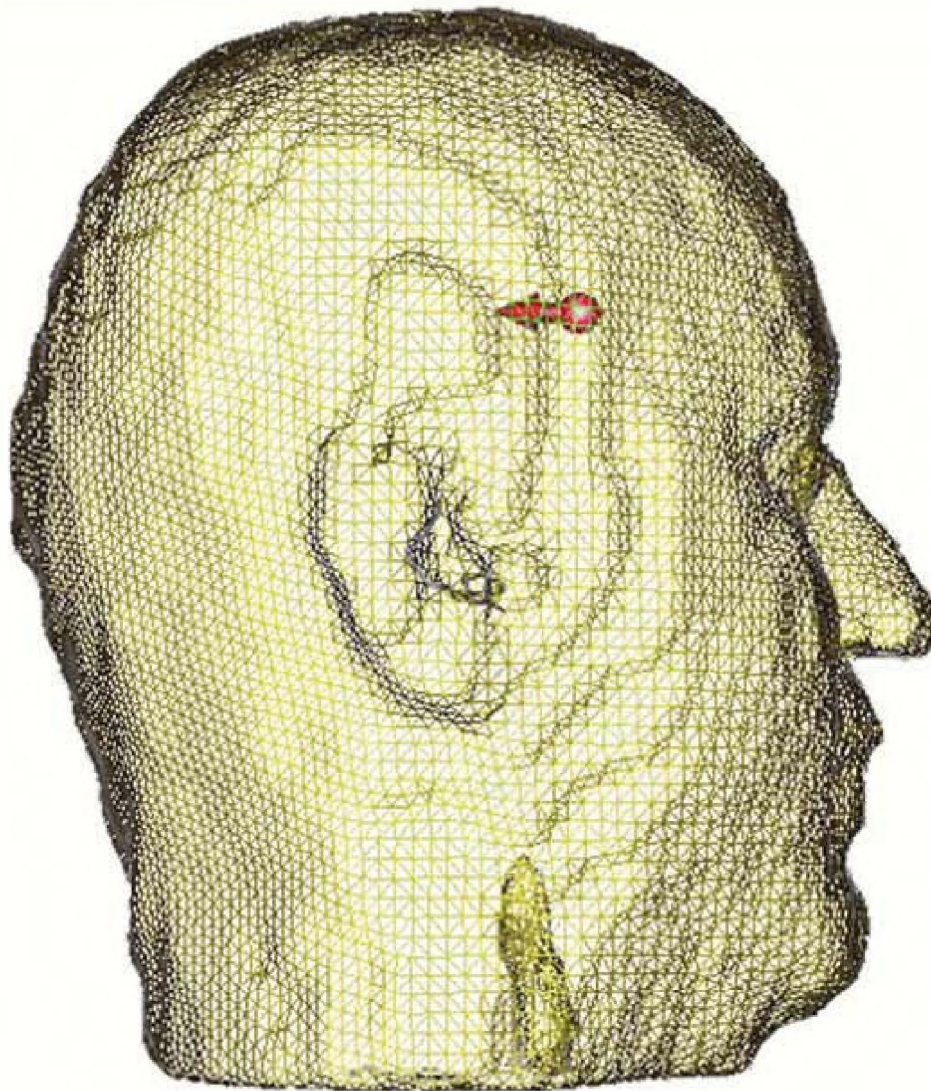


Figure 8: Dipole location calculated by inverse MEG simulation using "measured" data obtained from dipole positioned at (79,177,131) in the right posterior frontal area

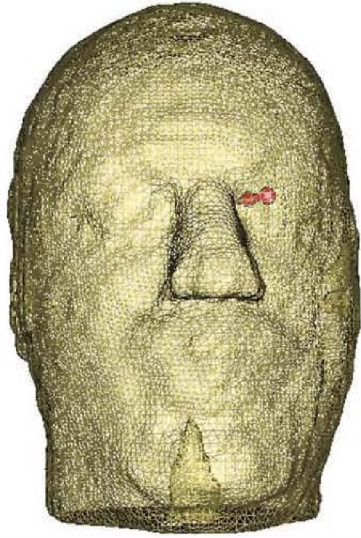


Figure 9: Dipole location calculated by inverse MEG simulation using “measured” data obtained from dipole positioned at (150,150,50) in the left parietal area, using magnetic fields due to both primary and volume currents

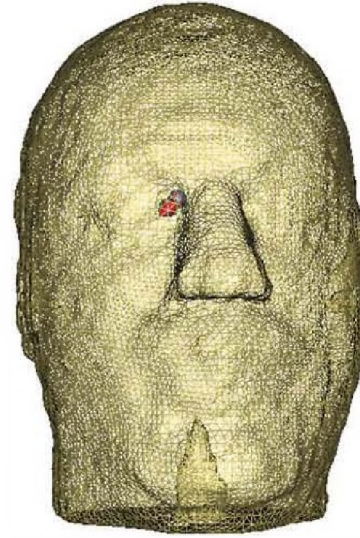


Figure 10: Dipole location calculated by inverse MEG simulation using “measured” data obtained from dipole positioned at (150,150,50) in the left parietal area, using magnetic fields due to primary currents alone

in Figure 6, calculations using both the volume and primary currents yielded a result closer to the expected near zero field strength than do calculations using primary currents alone. In Figure 7, detectors remote from the dipole location, such as detector numbers 37-51, generally have positive magnetic fields due to volume currents and negative fields resulting from primary currents. If the volume currents were not included in the calculation for these detectors, the total magnetic field measured at these detectors would appear to be negative rather than close to zero as would be expected for detectors in the right frontal region of the brain and a left parietal dipole.

Ten inverse simulations performed on the same “measured” data but with different starting points were performed to demonstrate that our inverse model works accurately and could consistently find the same solution regardless of the initial placement of the test dipole in the inverse downhill simplex simulation. This fact was demonstrated by the simulation correctly identifying the dipole position within an average error of 4.0 ± 5.1 mm with 90% of the simulations localizing the dipole source to within 5mm of the correct location and one simulation being as close as 0mm. A large error (18mm) occurred only in one trial in which the downhill simplex method localized a result to a relative, rather than an absolute, minimum in its calculations.

The inverse MEG simulations with dipoles at various positions within the realistic head model reemphasize the importance of including the magnetic field due to volume currents in calculations designed for dipole source localization. 70% of the localizations performed without using the magnetic field due to volume currents obtained a solution inaccurate by 7mm or greater, whereas 90% of the localizations performed including the magnetic fields due to both the primary and volume currents were within 6mm of the correct dipole location. Indeed, two simulations not using volume currents inaccurately localized the dipole to the wrong side of the head (trials 2 and 6 in Table 1). Figures 9 and 10 further il-

lustrate this point by showing trial number 2 where a dipole that should be localized to the left parietal lobe, as shown in Figure 9 from a simulation using the magnetic fields due to both primary and volume currents, was localized to the right frontal lobe (Figure 10) in a simulation which did not use the magnetic field due to volume currents. These results demonstrate that if the magnetic field due to the volume currents is not used in inverse simulations, dipole source localization may be very inaccurate. The necessity for including the magnetic field due to volume currents in inverse simulations in our model may seem obvious since the magnetic field due to volume currents was included in the forward simulation “measured” data. Yet, the importance of considering volume currents in inverse simulations is not diminished just because our model explicitly uses volume currents to calculate its “measured” data; Maxwell’s equations (1,2,3) and the Biot-Savart law (4), which are fundamental to describing the magnetic fields emanating from a dipole in any realistic head model, intrinsically consider the magnetic field due to volume currents. Indeed, as these equations similarly apply to neuronal activity in actual human brain, attempts to localize a neural dipole in a human brain from MEG data will require the use of the magnetic field due to volume currents in the calculations.

In homogeneous spheres, the contribution of volume currents to the magnetic field measured normal to the detectors may be ignored, but in any other situation the volume currents cannot be disregarded. The head is not a sphere, and the volume currents do effect the magnetic field measured by MEG in a realistic inhomogeneous model. The inclusion of the magnetic field due to volume currents gives more accurate solutions to the forward MEG problem and helps to more precisely localize neural sources in inverse MEG problems.

Future Work

In the near future, we plan to continue to investigate the importance of using realistic finite element head models, rather than spherical models, for forward and inverse MEG simulations. We also plan to study quantitatively the effect of various conductivity values within the head on normal components of the magnetic field as measured by MEG, and how these conductivities influence both forward and inverse MEG simulations.

Acknowledgments

This work was supported in part by the National Science Foundation, the Department of Energy, the National Institutes of Health, and the Utah State Centers of Excellence Program. The authors would like to thank Nathan Galli and Richard Coffey for their assistance in generating the figures.

References

- [1] D.S. Burnett. *Finite Element Analysis: From Concepts to Applications*. Addison-Wesley Publishing Company, 1987.
- [2] M.V.K. Chari and S.J. Salon. *Numeric Methods in Electromagnetism*. Academic Press, 2000.
- [3] R.M. Gulranjani. *Bioelectricity and Biomagnetism*. John Wiley & Sons, Inc., 1998.
- [4] M. Hämäläinen, R. Hari, R.J. Ilmoniemi, J. Knutila, and O.V. Lounasmaa. Magnetoencephalography - theory, instrumentation, and applications to noninvasive studies of the working human brain. *Rev. Modern Phys.*, 65:413–497, 1993.
- [5] J. Jin. *The Finite Element Method in Electromagnetics*. John Wiley & Sons, Inc., 1993.
- [6] J. Mahivuo and R. Plonsey. *Bioelectromagnetism*. Oxford University Press, 1995.
- [7] J.C. Mosher, R.M. Leahy, and P.S. Lewis. Matrix kernels for the forward problem in EEG and MEG. Technical report, Los Alamos Technical Report report LA-UR-97-3812, 1997.
- [8] J.C. Mosher, R.M. Leahy, and P.S. Lewis. EEG and MEG: Forward solutions for inverse methods. *IEEE Trans. Biomed. Eng.*, 46:245–259, 1999.
- [9] S.G. Parker, D.M. Weinstein, and C.R. Johnson. The SCIRun computational steering software system. In E. Arge, A.M. Bruaset, and H.P. Langtangen, editors, *Modern Software Tools in Scientific Computing*, pages 1–44. Birkhauser Press, 1997.
- [10] M.J. Peters and J.C. De Munck. The influence of model parameters on the inverse solution based on MEGs and EEGs. *Acta Otolaryngol.*, 491:61–69, 1991.
- [11] J. Savaras. Basic mathematical and electromagnetic concepts of the biomagnetic inverse problem. *Phys. Med. Biol.*, 32:11–22, 1987.
- [12] B. van den Broek. *Volume conduction effects in EEG and MEG*. PhD thesis, University of Twente, 1997.
- [13] D. Weinstein, L. Zhukov, and C. Johnson. Lead-field bases for electroencephalography source imaging. *Ann. Biomed. Eng.*, 28:1–7, 2000.
- [14] D.M. Weinstein and C.R. Johnson. Effects of geometric uncertainty on the inverse EEG problem. In R.L. Barbour, M.J. Carvlin, and M.A. Fiddy, editors, *Computational, Experimental, and Numerical Methods for Solving Ill-Posed Inverse Imaging Problems: Medical and Nonmedical Applications*, volume 3171, pages 138–145. SPIE, 1997.
- [15] L. Zhukov, D. Weinstein, and C. Johnson. Independent component analysis for EEG source localization. *IEEE Eng. Med. Biol. Mag.*, 19:87–96, 2000.
- [16] O.C. Zienkiewicz. *The Finite Element Method in Engineering Science*. McGraw-Hill, New York, 1977.